
Article:
Chan, H.-F. orcid.org/0000-0002-5382-2097, Smith, L.J. orcid.org/0000-0002-5769-423X, Biancardi, A.M. et al. (12 more authors) (2023) Image phenotyping of preterm-born children using hyperpolarised 129Xe lung MRI and multiple-breath washout. American Journal of Respiratory and Critical Care Medicine, 207 (1). pp. 89-100. ISSN 1073-449X

https://doi.org/10.1164/rccm.202203-0606oc

Image phenotyping of preterm-born children using hyperpolarised ^{129}Xe lung MRI and multiple-breath washout

Ho-Fung Chan[1], Laurie J. Smith[1], Alberto M. Biancardi[1], Jody Bray[1], Helen Marshall[1], Paul J.C. Hughes[1], Guilhem J. Collier[1], Madhwesha Rao[1], Graham Norquay[1], Andrew J. Swift[1], Kylie Hart[2,3], Michael Cousins[2,3], W. John Watkins[2], Jim M. Wild[1], Sailesh Kotecha[2,3]

[1]*POLARIS, Imaging Sciences, Department of Infection, Immunity and Cardiovascular Disease, University of Sheffield, Sheffield, United Kingdom*

[2]*Department of Child Health, Cardiff University School of Medicine, Cardiff, United Kingdom*

[3]*Neonatal Unit, Cardiff and Vale University Health Board, Cardiff, United Kingdom*

Corresponding Author: Professor Jim M. Wild

University MRI Unit, University of Sheffield, C Floor, Royal Hallamshire Hospital, Glossop Road, Sheffield, S10 2JF, UK. Email: j.m.wild@sheffield.ac.uk. Tel: +44 (0)114 215 9141

Author contributions:

SK and JW designed study; MC and KH recruited the children and conducted spirometry; HFC, LS, JB, GC, MR, GN and JW were responsible for MRI data acquisition; LS conducted multiple-breath washout testing; HFC, LS, AB, HM, PH, AS, WJW, JW, SK were responsible for the data analyses and interpretation; HFC, SK, JW and LS wrote the first draft of the manuscript which was subsequently commented on by all authors.

Funding sources: This work was supported by the Medical Research Council (MR/M008894/1 and MR/M022552/1) and National Institute for Health Research grant (NIHR-RP-R3-12-027). PH was funded by GlaxoSmithKline (BIDS3000032592). AS was funded by the Wellcome Trust (205188/Z/16/Z).

Running head: Hyperpolarised ^{129}Xe MRI and MBW in preterm-born children

Subject category: 14.03 Neonatal Lung Disease & BPD

Word count: 3500

Scientific Knowledge on the Subject

A common consequence after preterm birth is decreased lung function or prematurity-associated lung disease (PLD). PLD is commonly reported in preterm-born children who developed bronchopulmonary dysplasia (BPD) in infancy. Different phenotypes of PLD such as prematurity-associated obstructive lung disease (POLD) and prematurity-associated preserved ratio of impaired spirometry (pPRISm) may be associated with different early life factors and endotypes.

What This Study Adds to the Field

Hyperpolarised ^{129}Xe ventilation and diffusion-weighted MRI, and multiple breath washout (MBW) was used to assess the differential associations between the historical diagnosis of BPD and current lung function phenotypes on lung ventilation and microstructure in preterm-born children and term-born controls. Ventilation abnormalities from ^{129}Xe ventilation MRI and MBW were observed in the lungs of preterm-born children who have POLD, and abnormal alveolar dimensions from ^{129}Xe diffusion-weighted MRI were associated with preterm-born children who had BPD in infancy. ^{129}Xe MRI can be utilised to assess and

phenotype functional and microstructural abnormalities in the lungs of preterm-born children.

This article has an online data supplement, which is accessible from this issue's table of content online at www.atsjournals.org

Abstract

Rationale: Preterm birth is associated with low lung function in childhood, but little is known about the lung microstructure in childhood.

Objectives: We assessed the differential associations between the historical diagnosis of bronchopulmonary dysplasia (BPD) and current lung function phenotypes on lung ventilation and microstructure in preterm-born children using hyperpolarised ^{129}Xe ventilation and diffusion-weighted MRI, and multiple breath washout (MBW).

Methods: Data were available from 63 children (aged 9-13 years) including 44 born preterm (≤34 weeks' gestation) and 19 term-born controls (≥37 weeks' gestation). Preterm-born children were classified, using spirometry, into prematurity-associated obstructive lung disease (POLD, FEV_1<LLN, FEV_1/FVC<LLN); prematurity-associated preserved ratio of impaired spirometry (pPRISm, FEV_1<LLN, FEV_1/FVC≥LLN); preterm- and term-born controls; and into those with and without BPD. Ventilation heterogeneity metrics were derived from ^{129}Xe ventilation MRI and SF_6 MBW. Alveolar microstructural dimensions were derived from ^{129}Xe diffusion-weighted MRI.

Results: ^{129}Xe ventilation defect percentage and ventilation heterogeneity index were significantly increased in preterm-born children with POLD. In contrast, mean ^{129}Xe apparent diffusion coefficient (ADC), ^{129}Xe ADC interquartile range (IQR) and ^{129}Xe mean alveolar dimension IQR were significantly increased in preterm-born children with BPD, suggesting changes of alveolar dimensions. MBW metrics were all significantly increased in the POLD group when compared to preterm- and term-born controls. Linear regression confirmed the differential effects of obstructive disease on ventilation defects and BPD on lung microstructure.

Conclusion: We show that ventilation abnormalities are associated with prematurity-associated obstructive lung disease, and BPD in infancy is associated with abnormal lung microstructure.

Abstract length: 245 words

Keywords: Hyperpolarised ^{129}Xe MRI, bronchopulmonary dysplasia, multiple-breath washout, lung growth, lung function, chronic lung disease of prematurity, prematurity-associated lung disease.

Introduction

Decreased lung function (FEV_1<LLN) or prematurity-associated lung disease (PLD) is a common consequence after preterm birth. PLD is commonly reported in preterm-born children who developed bronchopulmonary dysplasia (BPD, also called chronic lung disease of prematurity, CLD) in infancy (1-3). Children born late-preterm at 33-36 weeks' gestation are also now recognized to be at risk of PLD in childhood and beyond (4, 5). Indeed, we recently showed that gestation and intrauterine growth restriction (IUGR) but not BPD were significantly associated with PLD in multivariable regression models (6). Furthermore, it is likely that different phenotypes of PLD may be associated with different early life factors, such as BPD, IUGR, gestation, and may result in different endotypes (6). Most focus has been on those who develop prematurity-associated obstructive lung disease (POLD, FEV_1<LLN, FEV_1/FVC<LLN) (7), but preserved ratio of impaired spirometry (PRISm, FEV_1<LLN, $FEV_1/FVC \geq$LLN) has been recently shown to be associated with development of chronic obstructive pulmonary disease (COPD), cardiovascular disease and increased all-cause mortality (8, 9). Although PLD has been shown to be associated with decreased lung function, the different phenotypes of PLD including POLD and prematurity-associated PRISm (pPRISm) have been less well reported (6).

Magnetic resonance imaging (MRI) has emerged as a powerful tool for functional and structural assessment of paediatric lung diseases including the use of advanced methods such as ultra-short echo time (UTE) structural MRI and inhaled hyperpolarised gas functional MRI (10, 11). Hyperpolarised helium-3 (^3He) or xenon-129 (^{129}Xe) MRI provides 3D *in vivo* measurements of lung ventilation and microstructure through ventilation and diffusion-weighted imaging, respectively (12, 13). Hyperpolarised gas MRI is safe and well-tolerated in

children (14), and has demonstrated sub-clinical sensitivity with the detection of lung ventilation abnormalities in diseases such as cystic fibrosis (CF) (15-17), asthma (18), and primary ciliary dyskinesia (PCD) (19). There is, however, a paucity of MRI studies of lung disease in preterm-born children. To date, MRI studies have included structural proton UTE imaging, (20-25), ^{3}He diffusion-weighted MRI (26, 27) and dissolved ^{129}Xe gas transfer MRI (28) in preterm-born neonates and children with BPD, and dynamic contrast-enhanced lung perfusion MRI in adult preterm-born survivors (29). To our knowledge, to date, no studies with ^{129}Xe ventilation or diffusion-weighted MRI have been reported in the lungs of preterm-born children.

Multiple-breath washout (MBW) of inhaled inert gases (SF_6 or N_2) provides global measures of ventilation heterogeneity, which are sensitive to early lung disease in children with CF (30). Metrics derived from MBW, such as lung clearance index (LCI), phase-III slope in the conducting airways (S_{cond}), and acinar lung regions (S_{acin}) have demonstrated significant differences between preterm-born children including those who had BPD in infancy and term-born children (31-33), but this has not been consistently reported (34-36), most likely due to heterogeneous lung disease in preterm-born subjects. LCI measurements are likely to complement those findings from ^{129}Xe ventilation and diffusion-weighted MRI to assess the function and microstructure of the preterm lung.

In this study, we assessed the differential associations between the historical diagnosis of BPD and current lung function with lung ventilation and microstructure in preterm-born children using ^{129}Xe ventilation and diffusion-weighted MRI, and MBW, comparing results from term-

born children. Some of the results of this study has been previously reported in the form of abstracts (37, 38).

Methods

Study subjects

The Respiratory Health Outcomes in Neonates study (RHiNO, EudraCT: 2015-003712-20) is a comprehensive study of respiratory disease of preterm-born children (≤34 weeks' gestation) and term-born controls (≥37 weeks' gestation) from South Wales aged 7–12 years at enrolment, evaluating mechanisms (6), a randomised controlled trial (RCT) (39) and hyperpolarised ^{129}Xe MRI. Pre-bronchodilator spirometry was performed 2-3 months prior to the MRI scans; quality controlled as per guidelines (40), and reported against GLI reference equations (41). Details on study recruitment and spirometry are described in the online data supplement.

65 children, aged 9-13 years at time of MRI, comprising 24 who entered the RCT, 20 preterm with %FEV_1>85% and 21 term-controls underwent MRI scanning at University of Sheffield, UK (see Figure E1 in online data supplement for CONSORT diagram). The children were classified according to their spirometry: prematurity-associated obstructive lung disease (POLD, n=13, FEV_1<LLN, FEV_1/FVC<LLN); prematurity-associated PRISm (n=4, pPRISm, FEV_1<LLN, FEV_1/FVC≥LLN); preterm controls (PT_C, n=27, FEV_1>LLN); term-born controls (n=21) regardless of their spirometry. Information on early-life factors including gestational age, birthweight, diagnosis of BPD (according to National Institute of Child Health and Human Development criteria of oxygen supplementation at 28 days of age (42)), and IUGR were obtained from the

neonatal medical notes. IUGR was defined as <10th percentile for birthweight adjusted for sex and gestation using the LMS Growth program (Medical Research Council) (43). All children were free of respiratory infections for at least three weeks prior to the MRI visit. Ethical approval was obtained from the South-West Bristol Research Ethics Committee (15/SW/0289) and written informed consent/assent was obtained from the parents/children.

Hyperpolarised ^{129}Xe MRI

Hyperpolarised ^{129}Xe MRI was performed on a 1.5T (GE-HDx) scanner using a flexible transmit/receive quadrature vest coil (Clinical MR Solutions, Brookfield, WI). 3D ^{129}Xe lung ventilation and diffusion-weighted MRI was performed in separate breath-holds ranging from 10-16 seconds following inhalation of a gas mixture of ^{129}Xe and N_2 from functional residual capacity (FRC). Hyperpolarised ^{129}Xe was produced with an in-house (POLARIS, Sheffield, UK) regulatory licenced polariser (~25% polarisation (44)), and gas mixture volumes and ^{129}Xe doses were titrated according to the subjects' heights to account for differences in lung volume (Table E1). ^{129}Xe ventilation imaging was performed with a 3D balanced steady-state free precession sequence as described previously (45). ^{1}H images of the thorax were acquired with a spoiled gradient echo (SPGR) sequence for anatomical reference. ^{129}Xe diffusion-weighted MRI was acquired with a 3D multiple b-value SPGR sequence with compressed sensing under-sampling as described previously (46) with a ^{129}Xe diffusion time=8.5ms and b-values=[0,12,20,30]s/cm^2. Further details on ^{129}Xe diffusion-weighted parameters are reported in the online data supplement.

^{129}Xe ventilation and ^{1}H image pairs were segmented using a semi-automated method (47) to calculate the ventilated lung and thoracic cavity masks, respectively. These two

segmentations were used to derive the ventilation defect percentage (VDP) and ventilation heterogeneity index (VHI). VDP is the percentage of unventilated lung volume, and VHI is a measure of ventilation heterogeneity based upon the coefficient of variation of surrounding pixels (17). Under-sampled ^{129}Xe diffusion-weighted images were reconstructed, and voxel-wise maps of ADC and mean alveolar dimension (Lm_D) were derived from the stretched exponential model (SEM) of hyperpolarised gas diffusion in the lungs (48). ADC was calculated from a mono-exponential fit of the first two diffusion b-values (b=0,12 s/cm^2); while Lm_D was calculated from a SEM fit of all four b-values. The global mean and interquartile range (IQR) of all values were calculated from the respective ^{129}Xe ADC and Lm_D maps.

Multiple breath washout

Multiple breath washout (MBW) was performed a minimum of three times on the same day as ^{129}Xe MRI with a modified open-circuit Innocor (Innovision, Glamsbjerg, Denmark) and 0.2% SF_6 (49). Lung clearance index (LCI), S_{cond}, and S_{acin} were calculated from the average of at least two technically acceptable trials.

Statistical analyses

The lower limit of normal (LLN) of spirometry was defined as <-1.64 z-scores (41). For each ^{129}Xe MRI and MBW metric, the 95% upper limit value (mean+1.64SD) was calculated from the respective term-born control group as a threshold to evaluate abnormal metrics in the preterm-born children. One-way ANOVA with post-hoc Tukey's test for multiple comparisons was performed (GraphPad Prism 7.04, San Diego, CA). Univariable and multivariable linear regression modelling were performed (SPSS V23.0, IBM, Armonk, NY) to identify associations

between early life factors and ^{129}Xe MRI and MBW metrics in the preterm-born children only. P<0.05 was considered statistically significant.

Results

From the 65 children assessed, two term-born children were excluded as one had an upper respiratory tract infection at the time of MRI scanning; and the other due to a technical issue with the ^{129}Xe MRI coil. Thus, data were available from 19 term-born children and 44 preterm-born children (13 with POLD, 4 with pPRISm and 27 were PT_C). In addition, 11 preterm-born children had BPD in infancy. Participant demographics are shown in Table E2 and Table 1 summarises the ^{129}Xe MRI and MBW metrics for the lung function phenotype and BPD groups separately.

Significantly higher ^{129}Xe VDP (p=0.009, p=0.007), ^{129}Xe VHI (p=0.001, p=0.001), S_{cond} (p<0.001, p<0.001) and LCI (p<0.001, p=0.003) were observed in the POLD group when compared to the PT_C and term control groups, respectively (Figure 1). S_{cond} (p=0.015) was also significantly higher in the POLD group when compared to the pPRISm group, and S_{acin} (p=0.024) was significantly higher in the POLD group when compared to the PT_C group only. There were no significant differences between the pPRISm, PT_C and term-control groups for any ^{129}Xe ventilation or MBW metrics. No significant differences between the lung function groups were observed for any ^{129}Xe DW-MRI metrics (Figure E2).

Representative ^{129}Xe ventilation images and 3D rendered ventilation videos from each group are shown in Figure 2 and Video E1-4 in the online data supplement, respectively. From the 13 POLD children, 6 (46%) had ^{129}Xe VDP greater than the 95% upper term-born control value

(VDP>1.16%) (dotted line in Figure 1A). For these 6 POLD subjects, ^{129}Xe VHI, S_{cond}, S_{acin}, and LCI were also elevated, with respect to the 95% upper term-born control values, in 5, 6, 2, and 5 of the subjects, respectively. The elevated ^{129}Xe VDP and VHI metrics in this subset of the POLD group were reflected in heterogeneous patterns in the ^{129}Xe ventilation images (Figure 2A). Conversely, the remaining 7 subjects in the POLD group did not exhibit patterns of ^{129}Xe ventilation heterogeneity despite having a significant obstructive pattern on spirometry (Figure 2B). ^{129}Xe ventilation images in the pPRISm, PT_C and term-born control groups all had a homogeneous pattern with low VDP and VHI values (Figure 2C-E).

When the BPD and no-BPD groups were compared, global mean ^{129}Xe ADC was significantly increased in the BPD group when compared to the no-BPD (p=0.034) and term-control (p=0.049) groups (Figure 3A). Similar trends were observed for global mean ^{129}Xe Lm_D, just failing to reach statistical significance on ANOVA (p=0.055). However, only 3 out of 11 children with BPD had global mean ^{129}Xe ADC and Lm_D values greater than the 95% upper term-born control value of ADC (>0.032 cm^2/s) and Lm_D (>270 μm) (dotted lines in Figure 3A-B). Significantly increased ^{129}Xe ADC and Lm_D IQR were observed in the BPD group when compared to both the no-BPD (p=0.003, p<0.001) and the term-born control (p<0.001, p<0.001) groups (Figure 3C-D). Within the BPD group, 6/11 and 7/11 children had ^{129}Xe ADC and Lm_D IQR, respectively, that was greater than the 95% upper term-born control value (ADC IQR>0.010 cm^2/s, Lm_D IQR>67 μm) (dotted lines in Figure 3C-D). There were no significant differences between the no-BPD and term-control groups for any ^{129}Xe diffusion-weighted metrics.

Representative ^{129}Xe ADC and Lm_D maps for each of the BPD groupings are shown in Figure 4. An increased number of elevated ADC or Lm_D regions were observed in the maps of the preterm-born subjects with BPD associated with increased alveolar airspace heterogeneity and elevated ^{129}Xe ADC or Lm_D IQR (Figure 4A). In contrast, representative ^{129}Xe ADC and Lm_D maps in the no-BPD and term-born control groups were less heterogeneous when compared to the BPD maps (Figure 4B-C). No significant differences were observed for any of the ^{129}Xe ventilation or MBW metrics between the BPD groupings (Figure E3).

Since both POLD and BPD groupings showed differential effects on the ventilation and microstructure metrics of the lung, we explored the associations of these two groupings as well as sex and IUGR with the various ^{129}Xe MRI and MBW metrics in a sub-group analysis of the preterm-born children only. Univariable analyses showed that sex was not associated with any MRI or MBW metrics, but IUGR was associated with ^{129}Xe ADC IQR, Lm_D IQR and S_{acin}. POLD was significantly associated with ^{129}Xe VDP, ^{129}Xe VHI, and all MBW metrics. In contrast, BPD was associated with all of the ^{129}Xe diffusion-weighted metrics (Table 2). These differential associations of POLD with ventilation parameters and BPD with microstructure remained unchanged when multiple variables with $p<0.10$, namely S_{acin}, ^{129}Xe ADC IQR and ^{129}Xe Lm_D IQR, were included in multivariable models (Table 3).

Discussion

By using hyperpolarised ^{129}Xe ventilation and diffusion-weighted MRI, alongside MBW, we report the differential effects of obstructive lung disease and BPD on functional and microstructural changes in the lungs of preterm-born children.

Increased ^{129}Xe ventilation metrics (VDP and VHI) were observed in some preterm-born children with reduced FEV_1 and obstructive pattern on spirometry (POLD) when compared to preterm-born children with preserved FEV_1 (PT_C) and term-born children. Although increased ^{129}Xe VDP and VHI have been reported in children with other obstructive lung diseases such as CF (17) and asthma (18), ^{129}Xe ventilation heterogeneity has not previously been reported in the preterm-born population. These data also demonstrate that most preterm-born children with preserved FEV_1 did not have ventilation abnormalities on MRI, with ^{129}Xe ventilation images generally resembling those observed in the term-born control children. The preterm-born children with preserved ratio of impaired spirometry (pPRISm) had findings similar to the two control groups but since only four subjects were available for study, the findings should be interpreted with caution.

Furthermore, within the POLD group, despite their $FEV_1 \leq LLN$, 7 of the 13 children (54%) did not have significant ventilation abnormalties on ^{129}Xe ventilation MRI (VDP<1.16%, the 95% upper term-born control value). This finding highlights significant discordance between the degree of impairment measured by FEV_1 and the ventilation images in preterm-born children with reduced lung function when compared to other paediatric airways disease. Studies of children with CF, PCD and asthma, for example, have all shown a strong correlation between low FEV_1 values and significant ventilation abnormalities (15-19). We have demonstrated here, however, that in preterm-born children with FEV_1 values as low as -3 z-scores, their ventilation images often appeared normal (Figure 2B). This suggests that the airflow obstruction has a different phenotype to those seen in subjects with ongoing lung disease progression such as in CF where active inflammation, infection and mucus plugging are

ongoing. In contrast, the remaining 6 POLD children demonstrated significant ventilation abnormalities that may highlight a phenotype whereby there is an ongoing active pathophysiological component to their airflow obstruction. Whether both or either group would benefit from inhaler treatment is speculative (39).

MBW metrics were consistent with the ^{129}Xe ventilation MRI measures, with trends towards increased S_{cond}, LCI, and S_{acin} observed in the POLD group when compared with the pPRISm, PT_C and term-born controls groups. In addition, similar to ^{129}Xe VDP and VHI, only a small subset of children in the POLD group had MBW metrics that were greater than those observed in the term-born control group. Significantly increased S_{cond} in the POLD group is in agreement with MBW measured with N_2 reported by Yammine and colleagues (32); however, the significantly elevated S_{acin} and LCI in the POLD group are contrary to what was observed in Yammine's study.

Increased LCI and S_{acin} in preterm-born children with or without BPD have previously been reported (31, 33), although other studies have not found any differences (34-36). In contrast, compared to previous studies (31, 33), in our study we did not find any differences for ^{129}Xe ventilation or MBW metrics between the BPD and no-BPD groups when compared to the term-born controls. Taken together, these observations suggest that prematurity-associated obstructive lung disease (POLD) can result in ventilation defects, and BPD affects lung microstructure.

The ^{129}Xe diffusion-weighted MRI measurements of acinar dimensions demonstrated increased global mean ^{129}Xe ADC alongside significantly elevated ^{129}Xe ADC and Lm_D IQR in

the BPD group when compared with the no-BPD and and term-born controls. Increased ^{129}Xe ADC and Lm_D IQR in the BPD group indicates regional heterogeneity in alveolar dimensions, which may result from preterm birth at an early stage of lung development especially in those born extremely preterm and/or due to neonatal interventions including mechanical respiratory support and increased supplemental oxygen. Visible regions of elevated values in ^{129}Xe ADC and Lm_D maps in some preterm born subjects with BPD (Figure 4A) illustrate this increased heterogeneity of alveolar dimensions. Furthermore, these subtle regional changes in alveolar dimensions go towards explaining why the IQR is a more sensitive metric than global mean in detecting alveolar dimension changes as a consequence of BPD in infancy.

The trends of increased and more heterogeneous ^{129}Xe diffusion-weighted MRI metrics in BPD from our study are in agreement with a previous ^{3}He diffusion-weighted MRI study by Flors et al. (26) where significantly increased ^{3}He ADC was observed in preterm-born children with BPD. The differences in diffusion metrics between term-born controls and children with BPD in our ^{129}Xe study were less striking than those observed in the Flors' study (26). This discrepancy could possibly be related to the fewer children with moderate/severe BPD in our ^{129}Xe study. Flors et al. (26) studied 16 subjects with moderate/severe BPD compared to 5 with mild BPD and 6 with moderate/severe BPD in our study. Furthermore, BPD subjects in our study were likely less severe as evidenced by only 3 subjects with global ^{129}Xe ADC and Lm_D greater than the 95% upper term-born control values.

Contrary to the trends observed in this work and the study by Flors et al. (26), the ^{3}He diffusion-weighted MRI study by Narayanan and colleagues (27) found no significant differences for ^{3}He ADC between children with BPD and term-born controls. However, the

longer diffusion times of the diffusion sequence used in that study may inherently sensitise those measurements to longer inter-acinar diffusion length-scales beyond alveolar dimensions (50). In addition, the spectroscopic acquisition used by Narayanan et al. only derived a global metric of alveolar dimensions, and therefore, was unable to measure more subtle regional heterogeneity differences in alveolar dimensions that were observed in our study with ^{129}Xe diffusion-weighted MRI.

In survivors of BPD, it has been demonstrated that lung function decline is present throughout childhood (51) and into adulthood (4), therefore, we speculate that those subjects in the preterm with BPD group, including those with normal alveolar dimensions as measured with ^{129}Xe MRI, may progress and exhibit more severe or elevated diffusion-weighted MRI metrics as the lung continues to develop into adulthood. This is supported by a small study of two adult survivors of BPD who demonstrated increased global mean ^{3}He ADC when compared to healthy adults of similar ages (52).

To further confirm that preterm-born children with low lung function were associated with ventilation heterogeneity, and the BPD group were associated with lung microstructure, we used univariable and multivariable linear regression analyses to investigate which early life factors, including sex, IUGR, BPD and spirometry, were most closely associated with ^{129}Xe MRI and MBW metrics. The multivariable regression results corroborated the findings observed after stratifying into low lung function groups and into BPD groups by reconfirming that all ^{129}Xe ventilation MRI and MBW metrics were significantly associated with a current obstructive pattern of lung disease; while ^{129}Xe diffusion-weighted metrics were significantly associated with a historical BPD diagnosis and the presence of IUGR. The ^{129}Xe diffusion

regression results also suggest that alterations in lung microstructure are associated with both antenatal (IUGR) and postnatal (supplemental oxygen, respiratory support) factors.

This study has several strengths and weaknesses. The strengths of the study are that we used two different methods, ^{129}Xe MRI and MBW, which both showed similar findings with regards to ventilation heterogeneity. Furthermore, ^{129}Xe MRI was able to demonstrate changes in regional ventilation and microstructural heterogeneity in the lungs of preterm-born children, that is not possible with conventional lung function tests. The sensitivity of ^{129}Xe diffusion-weighted MRI to lung microstructural changes is a particular strength especially with the paucity of histological or quantitative CT data available in the lungs of preterm-born children. We also assessed the role of important early life factors to demonstrate the differential effects of obstructive lung disease and BPD on ventilation and microstructure of the lung, respectively.

The weaknesses of the study are that we studied a relatively small number of subjects especially in some of the stratified groups, particularly the pPRISm group which should be interpreted with caution. Selection bias and recall bias given the small numbers may also be relevant. In addition, a wider range of gestation would have identified if the findings were associated with decreasing gestation and including greater numbers especially those with moderate/severe BPD would have strengthened our findings. A possible limitation for the acquisition of ^{129}Xe MRI is the absence of precise lung volume control that could affect derived ^{129}Xe MRI metrics. However, this was mitigated by coaching and practice bag inhalations prior to MRI scanning.

Conclusion

In conclusion, ^{129}Xe ventilation and MBW metrics were noted to be significantly increased in the lungs of preterm-born children who had prematurity-associated obstructive lung disease, POLD. In contrast, ^{129}Xe diffusion-weighted metrics were increased in preterm-born children who had BPD in infancy indicating alterations of alveolar dimensions. ^{129}Xe MRI can, therefore, be utilised to assess and phenotype functional and microstructural abnormalities in the lungs of preterm-born children.

Acknowledgements

The views expressed in this publication are those of the authors and not necessarily those of the NHS, the National Institute for Health Research and the Department of Health. We would like to acknowledge all members of the POLARIS research group at the University of Sheffield and the RHiNO team for their support. Finally, we would like to thank the children and their parents for their incredible enthusiasm and contribution for the study.

References

1. Doyle LW, Andersson S, Bush A, Cheong JLY, Clemm H, Evensen KAI, et al. Expiratory airflow in late adolescence and early adulthood in individuals born very preterm or with very low birthweight compared with controls born at term or with normal birthweight: a meta-analysis of individual participant data. *The Lancet Respiratory Medicine* 2019; 7(8): 677-686.
2. Kotecha SJ, Edwards MO, Watkins WJ, Henderson AJ, Paranjothy S, Dunstan FD, et al. Effect of preterm birth on later FEV1: a systematic review and meta-analysis. *Thorax* 2013; 68(8): 760-766.
3. Hurst JR, Beckmann J, Ni Y, Bolton CE, McEniery CM, Cockcroft JR, et al. Respiratory and Cardiovascular Outcomes in Survivors of Extremely Preterm Birth at 19 Years. *American Journal of Respiratory and Critical Care Medicine* 2020; 202(3): 422-432.
4. Bolton CE, Bush A, Hurst JR, Kotecha S, McGarvey L. Lung consequences in adults born prematurely. *Thorax* 2015; 70(6): 574-580.
5. Kotecha SJ, Watkins WJ, Paranjothy S, Dunstan FD, Henderson AJ, Kotecha S. Effect of late preterm birth on longitudinal lung spirometry in school age children and adolescents. *Thorax* 2012; 67(1): 54-61.
6. Hart K, Cousins M, Watkins WJ, Kotecha SJ, Henderson AJ, Kotecha S. Association of early-life factors with prematurity-associated lung disease: prospective cohort study. *Eur Respir J* 2022; 59(5).
7. Carraro S, Filippone M, Da Dalt L, Ferraro V, Maretti M, Bressan S, et al. Bronchopulmonary dysplasia: the earliest and perhaps the longest lasting obstructive lung disease in humans. *Early Hum Dev* 2013; 89 Suppl 3S3-5.
8. Marott JL, Ingebrigtsen TS, Colak Y, Vestbo J, Lange P. Trajectory of Preserved Ratio Impaired Spirometry: Natural History and Long-Term Prognosis. *Am J Respir Crit Care Med* 2021; 204(8): 910-920.
9. Wan ES, Balte P, Schwartz JE, Bhatt SP, Cassano PA, Couper D, et al. Association Between Preserved Ratio Impaired Spirometry and Clinical Outcomes in US Adults. *JAMA* 2021; 326(22): 2287-2298.
10. Woods JC, Wild JM, Wielputz MO, Clancy JP, Hatabu H, Kauczor HU, et al. Current state of the art MRI for the longitudinal assessment of cystic fibrosis. *J Magn Reson Imaging* 2020; 52(5): 1306-1320.
11. Tiddens H, Kuo W, van Straten M, Ciet P. Paediatric lung imaging: the times they are a-changin'. *Eur Respir Rev* 2018; 27(147): 170097.
12. Stewart NJ, Chan HF, Hughes PJC, Horn FC, Norquay G, Rao M, et al. Comparison of (3) He and (129) Xe MRI for evaluation of lung microstructure and ventilation at 1.5T. *J Magn Reson Imaging* 2018; 48(3): 632-642.
13. Chan HF, Collier GJ, Weatherley ND, Wild JM. Comparison of in vivo lung morphometry models from 3D multiple b-value (3) He and (129) Xe diffusion-weighted MRI. *Magn Reson Med* 2019; 81(5): 2959-2971.
14. Walkup LL, Thomen RP, Akinyi TG, Watters E, Ruppert K, Clancy JP, et al. Feasibility, tolerability and safety of pediatric hyperpolarized (129)Xe magnetic resonance imaging in healthy volunteers and children with cystic fibrosis. *Pediatr Radiol* 2016; 46(12): 1651-1662.
15. Marshall H, Horsley A, Taylor CJ, Smith L, Hughes D, Horn FC, et al. Detection of early subclinical lung disease in children with cystic fibrosis by lung ventilation imaging with hyperpolarised gas MRI. *Thorax* 2017; 72(8): 760-762.
16. Thomen RP, Walkup LL, Roach DJ, Cleveland ZI, Clancy JP, Woods JC. Hyperpolarized (129)Xe for investigation of mild cystic fibrosis lung disease in pediatric patients. *J Cyst Fibros* 2017; 16(2): 275-282.
17. Smith LJ, Collier GJ, Marshall H, Hughes PJC, Biancardi AM, Wildman M, et al. Patterns of regional lung physiology in cystic fibrosis using ventilation magnetic resonance imaging and multiple-breath washout. *Eur Respir J* 2018; 52(5): 1800821.
18. Cadman RV, Lemanske RF, Jr., Evans MD, Jackson DJ, Gern JE, Sorkness RL, et al. Pulmonary 3He magnetic resonance imaging of childhood asthma. *J Allergy Clin Immunol* 2013; 131(2): 369-376.

19. Smith LJ, West N, Hughes D, Marshall H, Johns CS, Stewart NJ, et al. Imaging Lung Function Abnormalities in Primary Ciliary Dyskinesia Using Hyperpolarized Gas Ventilation MRI. *Ann Am Thorac Soc* 2018; 15(12): 1487-1490.
20. Higano NS, Spielberg DR, Fleck RJ, Schapiro AH, Walkup LL, Hahn AD, et al. Neonatal Pulmonary Magnetic Resonance Imaging of Bronchopulmonary Dysplasia Predicts Short-Term Clinical Outcomes. *Am J Respir Crit Care Med* 2018; 198(10): 1302-1311.
21. Bates AJ, Higano NS, Hysinger EB, Fleck RJ, Hahn AD, Fain SB, et al. Quantitative Assessment of Regional Dynamic Airway Collapse in Neonates via Retrospectively Respiratory-Gated (1) H Ultrashort Echo Time MRI. *J Magn Reson Imaging* 2019; 49(3): 659-667.
22. Yoder LM, Higano NS, Schapiro AH, Fleck RJ, Hysinger EB, Bates AJ, et al. Elevated lung volumes in neonates with bronchopulmonary dysplasia measured via MRI. *Pediatr Pulmonol* 2019; 54(8): 1311-1318.
23. Hahn AD, Higano NS, Walkup LL, Thomen RP, Cao X, Merhar SL, et al. Pulmonary MRI of neonates in the intensive care unit using 3D ultrashort echo time and a small footprint MRI system. *J Magn Reson Imaging* 2017; 45(2): 463-471.
24. Katz SL, Parraga G, Luu TM, Santyr G, Abdeen N, Deschenes S, et al. Pulmonary Magnetic Resonance Imaging of Ex-preterm Children with/without Bronchopulmonary Dysplasia. *Ann Am Thorac Soc* 2022.
25. Forster K, Ertl-Wagner B, Ehrhardt H, Busen H, Sass S, Pomschar A, et al. Altered relaxation times in MRI indicate bronchopulmonary dysplasia. *Thorax* 2020; 75(2): 184-187.
26. Flors L, Mugler JP, 3rd, Paget-Brown A, Froh DK, de Lange EE, Patrie JT, et al. Hyperpolarized Helium-3 Diffusion-weighted Magnetic Resonance Imaging Detects Abnormalities of Lung Structure in Children With Bronchopulmonary Dysplasia. *J Thorac Imaging* 2017; 32(5): 323-332.
27. Narayanan M, Beardsmore CS, Owers-Bradley J, Dogaru CM, Mada M, Ball I, et al. Catch-up alveolarization in ex-preterm children: evidence from (3)He magnetic resonance. *Am J Respir Crit Care Med* 2013; 187(10): 1104-1109.
28. Willmering MM, Walkup LL, Niedbalski PJ, Wang H, Wang Z, Hysinger EB, et al. Pediatric (129) Xe Gas-Transfer MRI-Feasibility and Applicability. *J Magn Reson Imaging* 2022.
29. Barton GP, Torres LA, Goss KN, Eldridge MW, Fain SB. Pulmonary Microvascular Changes in Adult Survivors of Prematurity: Utility of Dynamic Contrast-enhanced Magnetic Resonance Imaging. *Am J Respir Crit Care Med* 2020; 202(10): 1471-1473.
30. Aurora P, Gustafsson P, Bush A, Lindblad A, Oliver C, Wallis CE, et al. Multiple breath inert gas washout as a measure of ventilation distribution in children with cystic fibrosis. *Thorax* 2004; 59(12): 1068-1073.
31. Sorensen JK, Buchvald F, Berg AK, Robinson PD, Nielsen KG. Ventilation inhomogeneity and NO and CO diffusing capacity in ex-premature school children. *Respir Med* 2018; 14094-100.
32. Yammine S, Schmidt A, Sutter O, Fouzas S, Singer F, Frey U, et al. Functional evidence for continued alveolarisation in former preterms at school age? *Eur Respir J* 2016; 47(1): 147-155.
33. Lum S, Kirkby J, Welsh L, Marlow N, Hennessy E, Stocks J. Nature and severity of lung function abnormalities in extremely pre-term children at 11 years of age. *Eur Respir J* 2011; 37(5): 1199-1207.
34. Hulskamp G, Lum S, Stocks J, Wade A, Hoo AF, Costeloe K, et al. Association of prematurity, lung disease and body size with lung volume and ventilation inhomogeneity in unsedated neonates: a multicentre study. *Thorax* 2009; 64(3): 240-245.
35. Latzin P, Roth S, Thamrin C, Hutten GJ, Pramana I, Kuehni CE, et al. Lung volume, breathing pattern and ventilation inhomogeneity in preterm and term infants. *PLoS One* 2009; 4(2): e4635.
36. Yaacoby-Bianu K, Plonsky MT, Gur M, Bar-Yoseph R, Kugelman A, Bentur L. Effect of late preterm birth on lung clearance index and respiratory physiology in school-age children. *Pediatr Pulmonol* 2019; 54(8): 1250-1256.

37. Wild JM, Biancardi A, Chan H-F, Smith L, Bray J, Marshall H, et al. Imaging functional and microstructural changes in the lungs of children born prematurely. *European Respiratory Journal* 2019; 54(suppl 63): PA3171.
38. Wild JM, Biancardi A, Chan H-F, Smith L, Bray J, Marshall H, et al. Imaging functional and microstructural changes in the lungs of children born prematurely. *Proc Intl Soc Mag Reson Med* 2019; 27(4083).
39. Goulden N, Cousins M, Hart K, Jenkins A, Willetts G, Yendle L, et al. Inhaled Corticosteroids Alone and in Combination With Long-Acting beta2 Receptor Agonists to Treat Reduced Lung Function in Preterm-Born Children: A Randomized Clinical Trial. *JAMA Pediatr* 2022; 176(2): 133-141.
40. Miller MR, Hankinson J, Brusasco V, Burgos F, Casaburi R, Coates A, et al. Standardisation of spirometry. *Eur Respir J* 2005; 26(2): 319-338.
41. Quanjer PH, Stanojevic S, Cole TJ, Baur X, Hall GL, Culver BH, et al. Multi-ethnic reference values for spirometry for the 3-95-yr age range: the global lung function 2012 equations. *Eur Respir J* 2012; 40(6): 1324-1343.
42. Jobe AH, Bancalari E. Bronchopulmonary dysplasia. *Am J Respir Crit Care Med* 2001; 163(7): 1723-1729.
43. Pan H, Cole T. LMSgrowth, a Microsoft Excel add-in to access growth references based on the LMS method. 2012.
44. Norquay G, Collier GJ, Rao M, Stewart NJ, Wild JM. ^{129}Xe-Rb Spin-Exchange Optical Pumping with High Photon Efficiency. *Phys Rev Lett* 2018; 121(15): 153201.
45. Stewart NJ, Norquay G, Griffiths PD, Wild JM. Feasibility of human lung ventilation imaging using highly polarized naturally abundant xenon and optimized three-dimensional steady-state free precession. *Magn Reson Med* 2015; 74(2): 346-352.
46. Chan HF, Stewart NJ, Norquay G, Collier GJ, Wild JM. 3D diffusion-weighted (129) Xe MRI for whole lung morphometry. *Magn Reson Med* 2018; 79(6): 2986-2995.
47. Hughes PJC, Horn FC, Collier GJ, Biancardi A, Marshall H, Wild JM. Spatial fuzzy c-means thresholding for semiautomated calculation of percentage lung ventilated volume from hyperpolarized gas and (1) H MRI. *J Magn Reson Imaging* 2018; 47(3): 640-646.
48. Chan HF, Collier GJ, Parra-Robles J, Wild JM. Finite element simulations of hyperpolarized gas DWI in micro-CT meshes of acinar airways: validating the cylinder and stretched exponential models of lung microstructural length scales. *Magn Reson Med* 2021; 86(1): 514-525.
49. Horsley AR, Gustafsson PM, Macleod KA, Saunders C, Greening AP, Porteous DJ, et al. Lung clearance index is a sensitive, repeatable and practical measure of airways disease in adults with cystic fibrosis. *Thorax* 2008; 63(2): 135-140.
50. Parra-Robles J, Wild JM. On the use of 3He diffusion magnetic resonance as evidence of neo-alveolarization during childhood and adolescence. *Am J Respir Crit Care Med* 2014; 189(4): 501-502.
51. Simpson SJ, Turkovic L, Wilson AC, Verheggen M, Logie KM, Pillow JJ, et al. Lung function trajectories throughout childhood in survivors of very preterm birth: a longitudinal cohort study. *The Lancet Child & Adolescent Health* 2018; 2(5): 350-359.
52. Sheikh K, Bhalla A, Ouriadov A, Young HM, Yamashita CM, Luu TM, et al. Pulmonary magnetic resonance imaging biomarkers of lung structure and function in adult survivors of bronchopulmonary dysplasia with COPD. *Cogent Medicine* 2017; 4(1): 1282033.

	Preterm Lung Function Grouping			Term Controls	Preterm BPD Grouping	
	POLD	pPRISm	PT_C		BPD	No BPD
Subjects (% total)	13 (21%)	4 (6%)	27 (43%)	19 (30%)	11 (17%)	33 (52%)
Sex (M:F)	4:9	1:3	11:16	9:10	4:7	12:21
Age (years)	11.7 (1.0)	11.4 (1.6)	11.7 (1.0)	10.6 (1.1)	11.6 (0.7)	11.6 (1.1)
Height (cm)	144.7 (9.5)	150.8 (18.6)	150.2 (10.7)	143.5 (9.8)	146.0 (11.8)	149.5 (11.0)
Weight (kg)	37.7 (12.4)	44.9 (16.9)	40.6 (11.4)	36.9 (12.6)	39.5 (15.1)	40.4 (11.2)
Gestational Weeks	29 (2)	30 (3)	31 (3)	40 (1)	27 (2)	31 (2)
BPD	5/13 (38%)	1/4 (25%)	5/27 (19%)	N/A	11/11 (100%)	0/33 (0%)
Mild BPD	1/13 (8%)	1/4 (25%)	3/27 (11%)	N/A	5/11 (45%)	-
Moderate/Severe BPD	4/13 (31%)	0/4 (0%)	2/27 (7%)	N/A	6/11 (55%)	-
FEV_1 (z-scores)	-2.97 (0.66)	-1.99 (0.26)	-0.38 (0.94)	0.32 (0.46)	-1.61 (1.75)	-1.19 (1.34)
FEV_1 (%predicted)	64.5 (8.2)	76.5 (3.1)	95.3 (10.6)	103.9 (6.5)	80.7 (20.5)	85.7 (15.7)
FVC (z-scores)	-0.54 (0.78)	-1.77 (0.30)	0.10 (0.99)	0.50 (0.59)	-0.27 (1.20)	-0.25 (1.00)
FVC (%predicted)	93.7 (9.0)	79.5 (3.5)	100.7 (11.1)	106.1 (6.8)	96.8 (13.9)	96.7 (11.2)
FEV_1/FVC (z-scores)	-3.14 (0.56)	-0.63 (0.46)	-0.78 (1.01)	-0.34 (0.86)	-1.83 (1.41)	-1.35 (1.38)
FEV_1/FVC (%predicted)	68.6 (8.8)	95.7 (3.2)	94.1 (7.7)	97.3 (5.4)	82.7 (15.4)	88.0 (13.6)
^{129}Xe VDP (%)	2.51 (3.56)	0.99 (1.04)	0.57 (0.75)	0.41 (0.46)	1.13 (1.64)	1.22 (2.38)
^{129}Xe VHI (%)	9.92 (2.31)	8.37 (0.80)	7.92 (1.35)	7.81 (1.05)	8.40 (2.08)	8.63 (1.82)
Mean ^{129}Xe ADC (cm^2/s)	0.0288 (0.0046)	0.0276 (0.0029)	0.0271 (0.0025)	0.0269 (0.0029)	0.0298 (0.0044)	0.0270 (0.0026)
^{129}Xe ADC IQR (cm^2/s)	0.0101 (0.0022)	0.0095 (0.0004)	0.0095 (0.0018)	0.0086 (0.0009)	0.0111 (0.0024)	0.0092 (0.0014)
Mean ^{129}Xe Lm_D (µm)	252 (23)	246 (15)	244 (13)	244 (16)	257 (22)	243 (14)
^{129}Xe Lm_D IQR (µm)	66 (8)	67 (4)	63 (9)	59 (5)	72 (9)	62 (7)
LCI	7.09 (1.55)	6.09 (0.11)	6.03 (0.42)	6.07 (0.28)	6.48 (0.98)	6.30 (1.03)
S_{cond} (L^{-1})	0.046 (0.025)	0.018 (0.007)	0.023 (0.012)	0.022 (0.014)	0.030 (0.022)	0.030 (0.020)
S_{acin} (L^{-1})	0.119 (0.049)	0.069 (0.044)	0.083 (0.028)	0.092 (0.034)	0.110 (0.047)	0.087 (0.037)

Abbreviations: POLD = prematurity-associated obstructive lung disease ($FEV_1 \leq LLN$, $FEV_1/FVC \leq LLN$); pPRISm = prematurity-associated preserved ratio of impaired spirometry ($FEV_1 \leq LLN$, $FEV_1/FVC > LLN$); PT_C = preterm with normal lung function ($FEV_1 > LLN$); BPD = preterm with bronchopulmonary dysplasia (BPD) diagnosis; VDP = ventilation defect percentage; VHI = ventilation heterogeneity index; ADC = apparent diffusion coefficient; IQR = interquartile range; Lm_D = mean alveolar dimension; LCI = lung clearance index.

Table 1: Summary of subject demographics, and metrics from spirometry, ^{129}Xe MRI and MBW for each grouping of preterm-born children based on either current lung function or historical diagnosis of BPD and term-born controls. All values are given as mean (standard deviation).

Factors			^{129}Xe VDP	^{129}Xe VHI	S_{cond}	S_{acin}	LCI	^{129}Xe ADC Mean	^{129}Xe ADC IQR	^{129}Xe Lm_D Mean	^{129}Xe Lm_D IQR
Sex (ref = male)		Beta	-0.321	-0.098	-0.006	-0.012	-0.336	0.002	0	7.412	1.317
		SE	0.683	0.582	0.006	0.308	0.308	0.001	0.001	5.17	2.577
		95% CI	-1.66,1.02	-1.24,1.04	-0.02,0.01	-0.62,0.59	-0.94,0.27	0,0.004	-0.002,0.002	-2.72,17.55	-3.73,6.37
		p-value	0.638	0.866	0.348	0.317	0.275	0.121	0.692	0.152	0.609
IUGR (ref = no IUGR)		Beta	0.111	0.136	0.013	0.042	0.548	0.001	0.002	6.927	7.638
		SE	0.955	0.811	0.008	0.016	0.429	0.001	0.001	7.202	3.359
		95% CI	-1.76,1.98	-1.45,1.73	0,0.03	0.01,0.07	-0.29,1.39	-0.001,0.003	0,0.004	-7.19,21.04	1.05,14.22
		p-value	0.908	0.867	0.108	**0.010***	0.202	0.312	**0.002***	0.336	**0.023***
Preterm lung function (ref = PT_C)	**POLD**	Beta	1.936	1.997	0.023	0.036	1.064	0.002	8.094	0.001	2.454
		SE	0.675	0.547	0.006	0.012	0.294	0.001	5.604	0.001	2.767
		95% CI	0.61,3.26	0.92,3.07	0.01,0.03	0.01,0.06	0.49,1.64	0,0.004	-2.89,19.08	-0.001,0.003	-2.97,7.88
		p-value	**0.004***	**0.000***	**0.000***	**0.003***	**0.000***	0.126	0.149	0.27	0.375
	pPRISm	Beta	0.413	0.445	-0.006	-0.014	0.063	0.001	2.061	0	3.187
		SE	1.067	0.865	0.009	0.019	0.467	0.002	8.653	0.001	4.272
		95% CI	-1.68,2.5	-1.25,2.14	-0.02,0.01	-0.05,0.02	-0.85,0.98	-0.003,0.005	-14.9,19.02	-0.002,0.002	-5.19,11.56
		p-value	0.699	0.607	0.514	0.451	0.892	0.755	0.812	0.998	0.456
BPD (ref = no BPD)		Beta	-0.09	-0.227	0.001	0.023	0.182	0.003	0.002	13.735	9.65
		SE	0.758	0.644	0.007	0.013	0.346	0.001	0.001	5.591	2.52
		95% CI	-1.58,1.40	-1.49,1.04	-0.01,0.01	0,0.05	-0.5,0.86	0.001,0.005	0,0.004	2.78,24.69	4.71,14.59
		p-value	0.905	0.724	0.921	0.091	0.598	**0.010***	**0.002***	**0.014***	**0.000***

Table 2: Summary of univariable linear regression analyses of ^{129}Xe MRI and MBW metrics in the preterm-born children only. Statistically significant factors related to early life (sex, BPD diagnosis, IUGR) and reduced lung function on spirometry are indicated in bold.

Factors			S_{acin}	^{129}Xe ADC IQR	^{129}Xe Lm_D IQR
IUGR (ref = no IUGR)		Beta SE 95% CI p-value	0.028 0.016 -0.003,0.06 0.079	0.002 0.001 0,0.004 **0.010***	4.961 3.082 -1.08,11 0.107
Preterm lung function (ref = PT_C)	**POLD**	Beta SE 95% CI p-value	0.029 0.012 0.01,0.05 **0.016***	-	-
	pPRISm	Beta SE 95% CI p-value	-0.012 0.018 -0.05,0.02 0.508	-	-
BPD (ref = no BPD)		Beta SE 95% CI p-value	-	0.002 0.001 0,0.004 **0.008***	8.613 2.528 3.66,13.57 **0.001***

Table 3: Summary of multivariable linear regression analyses of ^{129}Xe MRI and MBW metrics in the preterm-born children only. Statistically significant factors related to BPD diagnosis, IUGR and reduced lung function on spirometry are indicated in bold.

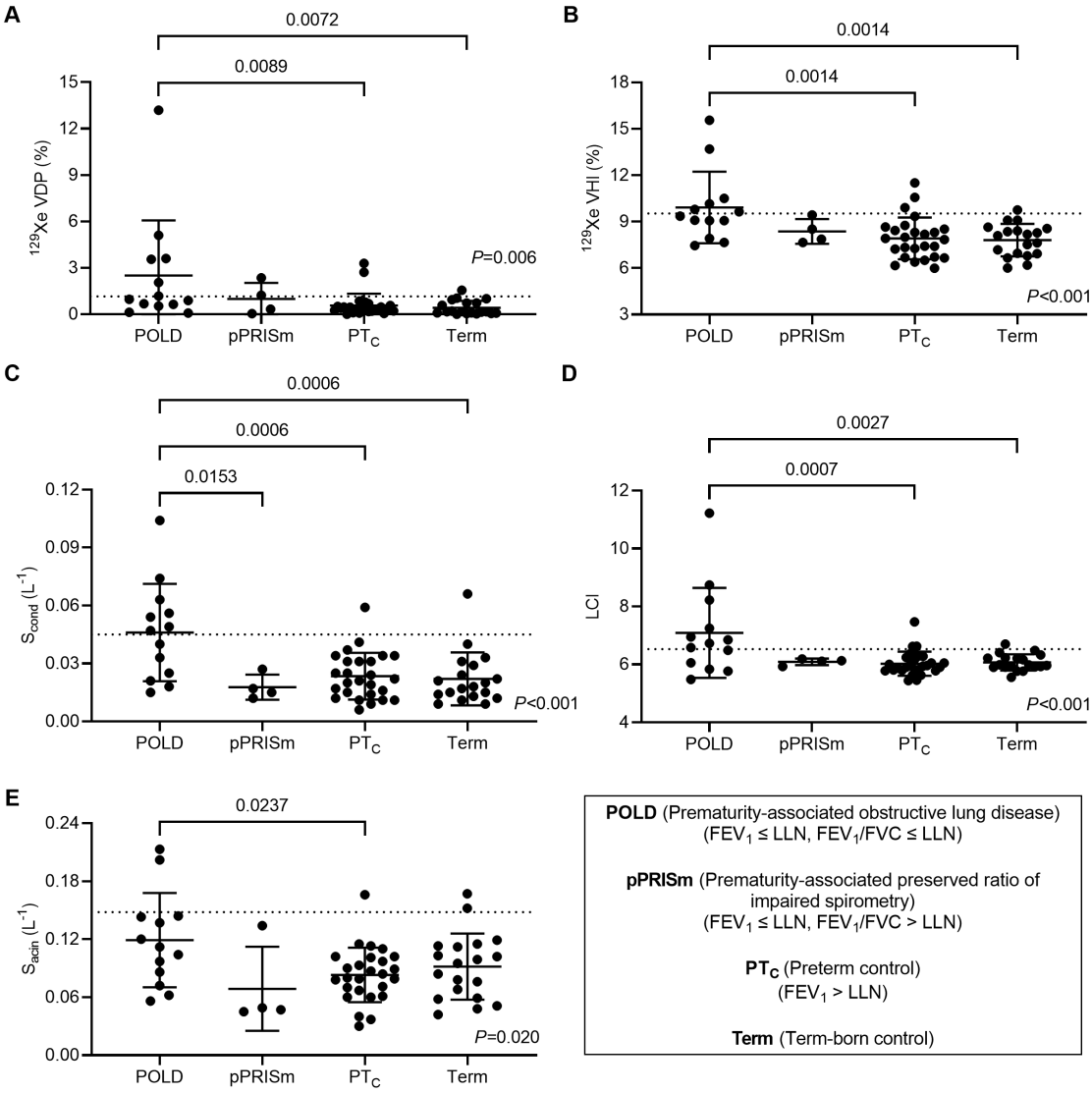

Figure 1: Plots of ^{129}Xe ventilation defect percentage (VDP) (A), ^{129}Xe ventilation heterogeneity index (VHI) (B), S_{cond} (C), S_{acin} (D), and lung clearance index (LCI) (E) for preterm-born children lung function phenotypes and term-born children. All plots have mean and standard deviation bars and p-values from ANOVA tests (boxed p-value is for Tukey's multiple comparison tests between groups). Dotted lines represent 95% upper limit of each ^{129}Xe MRI or MBW metric calculated from the term-born children group.

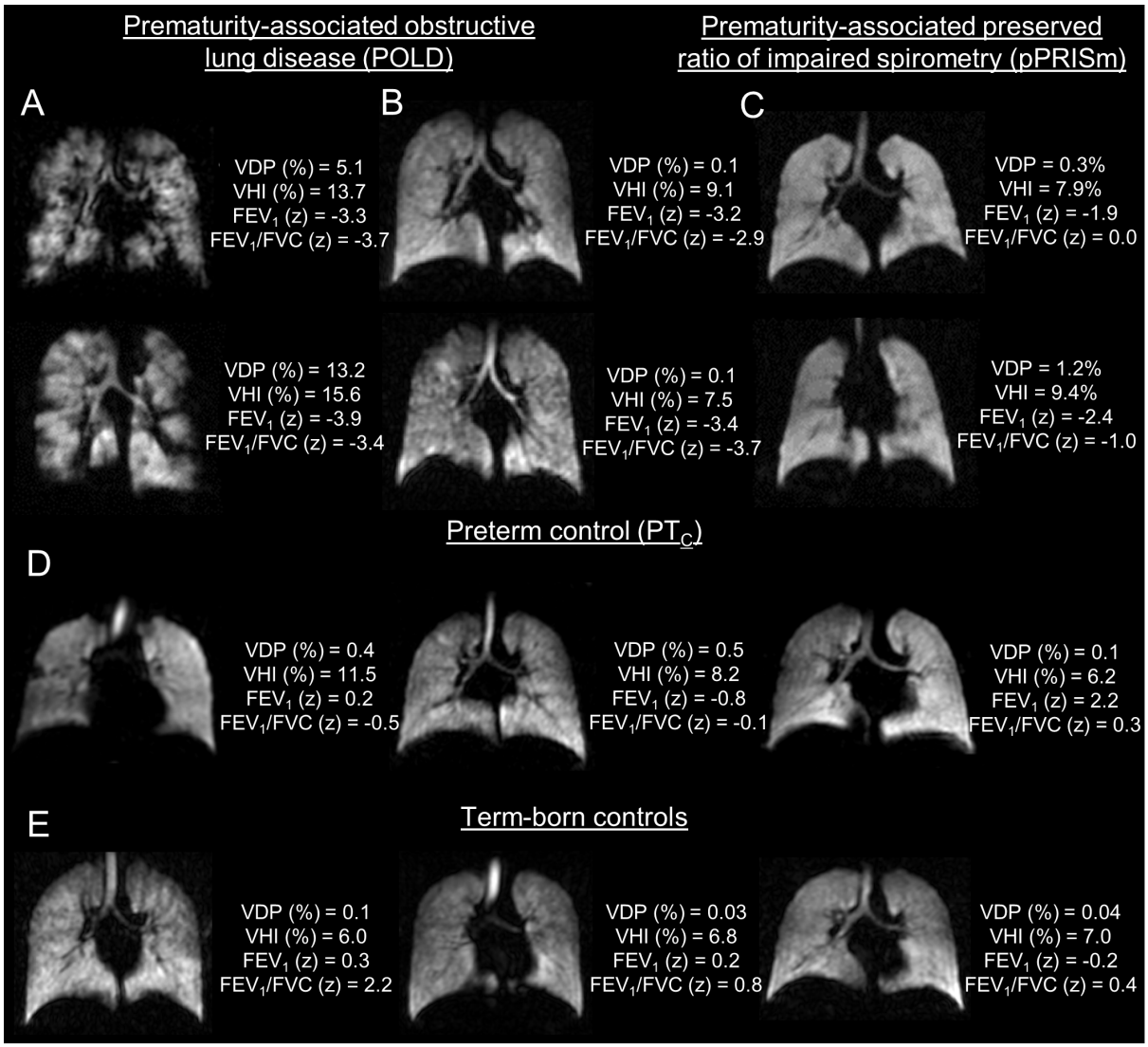

Figure 2: Representative single slice ^{129}Xe ventilation MR images from each preterm lung function phenotype group and term-born children. (A) POLD subjects with elevated ventilation MRI metrics, (B) POLD subjects with ventilation MRI metrics within the normal range. (C-E) pPRISm, PT_C and term-born control subjects with ventilation MRI metrics within the normal range.

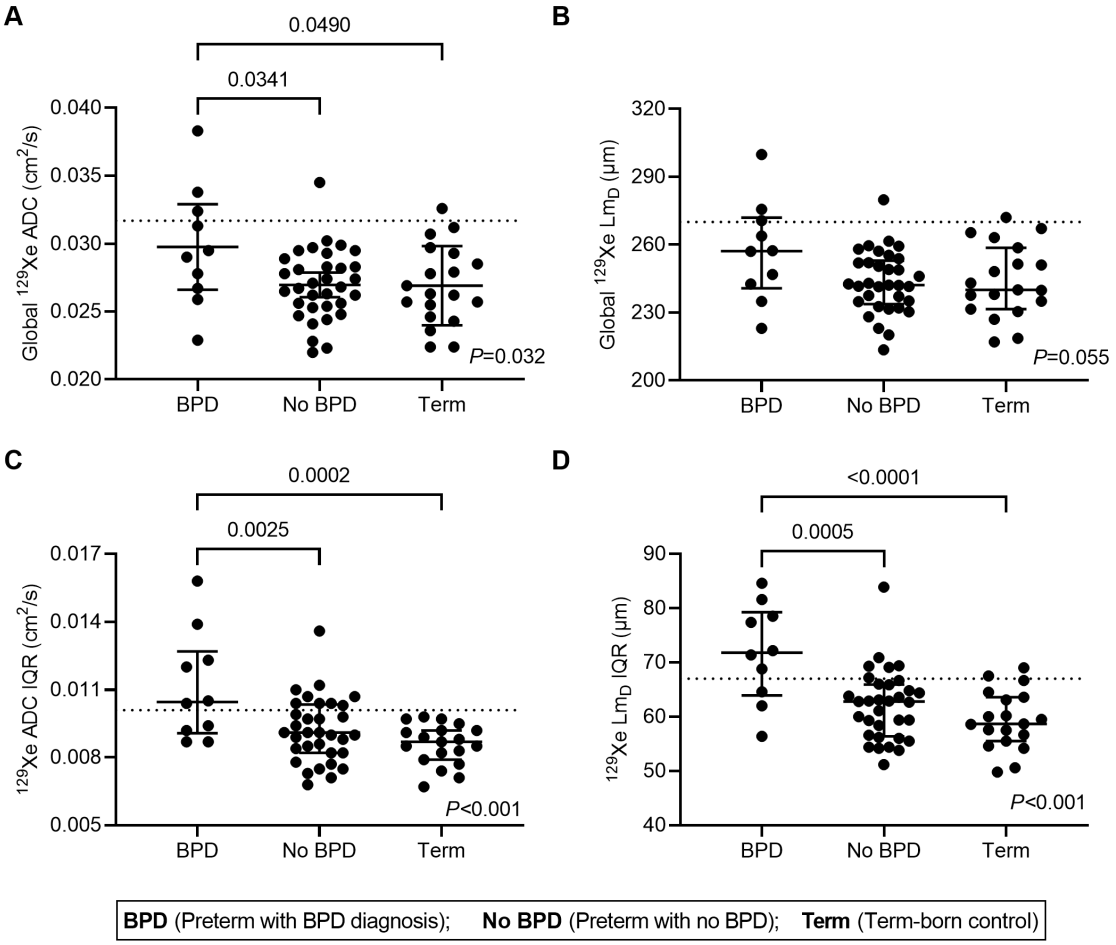

Figure 3: Plots of ^{129}Xe global mean apparent diffusion coefficient (ADC) (A), ^{129}Xe global mean alveolar dimension (Lm_D) (B), ^{129}Xe ADC interquartile range (IQR) (C), and ^{129}Xe Lm_D IQR (D) for preterm-born children grouped by BPD diagnosis and term-born children. All plots have mean and standard deviation bars and p-values from ANOVA tests (boxed p-value is for Tukey's multiple comparison tests between groups). Dotted lines represent 95% upper limit of each ^{129}Xe diffusion-weighted MRI metric calculated from the term-born children group.

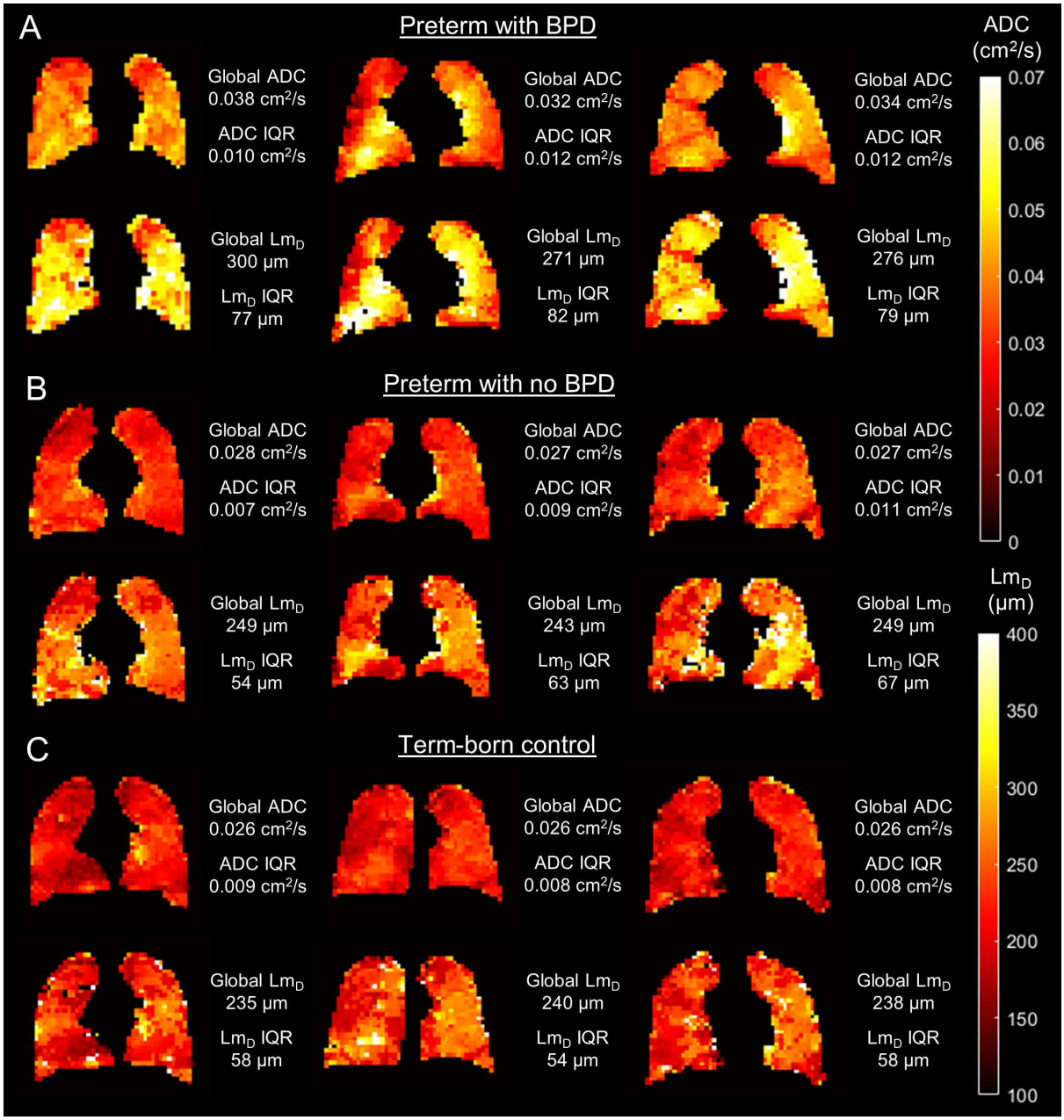

Figure 4: Representative single slice ^{129}Xe diffusion-weighted MRI derived maps of apparent diffusion coefficient (ADC) and mean alveolar dimension (Lm_D) of three different subjects from each BPD diagnosis grouping and term-born children.